CHINESE JOURNAL OF PHYSICS VOL. 52, NO. 1-II February 2014

Review

High-Order Harmonic Generation Driven by Two-Color Laser Fields

Guihua Li,[1,2] Jinping Yao,[1,*] Chaojin Zhang,[1,3] Bin Zeng,[1] Wei Chu,[1] Jielei Ni,[1] Jing Chen,[4,5] Zhinan Zeng,[1] Ruxin Li,[1] Ya Cheng,[1] and Zhizhan Xu[1]

[1]*State Key Laboratory of High Field Laser Physics, Shanghai Institute of Optics and Fine Mechanics, Chinese Academy of Sciences, Shanghai 201800, China*
[2]*University of Chinese Academy of Sciences, Beijing 100049, China*
[3]*School of Physics and Electronic Engineering, Jiangsu Normal University, Xuzhou 221116, China*
[4]*Key Laboratory of High Energy Density Physics Simulation, Center for Applied Physics and Technology, Peking University, Beijing 100084, China*
[5]*Institute of Applied Physics and Computational Mathematics, Beijing 100088, China*
(Received November 2, 2013)

In the past three decades, high-order harmonic generation (HHG) has attracted much attention due to its promising applications on creating table-top coherent extreme-ultraviolet (EUV/XUV) or X-ray sources, synthesizing attosecond pulses, probing electron dynamics and making "molecular movies", etc. We review our recent experimental and theoretical progresses in HHG driven by two-color laser fields, including broadening of XUV supercontinuum, generation of isolated attosecond pulses (IAPs), selection of long or short quantum trajectories, enhancement of HHG yield, creation of wavelength-tunable, bandwidth-controlled XUV emission, etc.

DOI: 10.6122/CJP.52.366 PACS numbers: 42.65.Ky, 42.65.Re

I. INTRODUCTION

In the past three decades, significant advances in high-order harmonic generation (HHG) have opened up a wide range of potential research opportunities in physics, biology, chemistry, material science, etc. From the well-known simple-man model [1], HHG can be intuitively understood as the subsequence of three steps. The electron first tunnels through the barrier formed by the combined action of Coulomb potential and the driving laser field (ionization), then it oscillates in the laser field (propagation), and finally it may recombine with the parent ion and emit a photon with an energy equal to the ionization potential plus the kinetic energy obtained from the laser field (recombination). In this way, HHG provides table-top ultrafast extreme-ultraviolet (EUV/XUV) or X-ray sources with high temporal and spatial coherence, which not only motivates its potential applications on

*Electronic address: jinpingmrg@163.com

 © 2014 THE PHYSICAL SOCIETY OF THE REPUBLIC OF CHINA

nanolithography [2], high-contrast X-ray microscopy [3], ultrafast electron spectroscopy [4–6], bio-imaging [7, 8] and so on, but also paves a way for spanning from femtosecond chemistry to attosecond physics [9]. Furthermore, the inherent pump-probe property during HHG process makes itself a tool for investigation of light-matter interaction in the strong field regime. For example, we can retrieve the information of molecular structures [10, 11] and dynamics [12–14] from HHG, which makes an important step towards the dream of making "molecular movies" with attosecond temporal and sub-angstrom spatial resolutions.

Based on the expectations mentioned above, considerable efforts have been devoted to extending the cutoff energy of HHG, improving HHG yield, shortening the duration of isolated attosecond pulses (IAPs), controlling XUV or X-ray emission (e.g., polarization, central wavelength and bandwidth, etc.). It is well known from the simple-man model [1] that the three processes involved in HHG all depend strongly on the waveform of the driving laser field, which offers us an opportunity to manipulate HHG as well as electron wavepacket dynamics with a great flexibility. A simple, straightforward method to waveform shaping is to control carrier-envelop phase (CEP) of few-cycle laser pulses [15]. However, the creation of few-cycle, high-energy laser pulses is now still a challenge for most laboratories; on the other hand, the limited waveform-control capability makes this approach difficult to enable a full control of HHG. Another technique is to tailor the shape of driving pulses with sub-cycle resolution and attosecond precision by a 1.5-octave three-channel optical field synthesizer and their attosecond sampling [16]. However, the employment of sophisticated waveform tailoring system often leads to increased complexity of the experimental setup, limited driving pulse energies, and extra optical losses. Two-color field technique [17–19] effectively combines the advantages of two methods as we will show below. It is not only simple but also highly flexible for experimental implementation.

The review focuses on the generation and manipulation of high-order harmonics in a two-color laser field. We firstly give an intuitive picture on manipulation of HHG with a two-color laser field. And then we will discuss the advantages of two-color field scheme on broadening of XUV supercontinuum, shorter attosecond pulse generation, selection of long or short quantum trajectories, enhancement of HHG yield, and the creation of wavelength-tunable, bandwidth-controlled XUV emission due to its ability of sub-cycle control for electron wavepackets. Finally, we give a summary and the future outlook about HHG in the two-color field.

II. MANIPULATION OF HHG WITH A TWO-COLOR LASER FIELD

The key point of manipulating HHG with a two-color laser field is to control the electron wavepacket dynamics, including tunnel ionization of electron, propagation of electron in the laser field and its recombination with parent ions. In this section, we will provide a basic picture on how two-color laser field affects three processes above.

First, tunnel ionization, as the first step as well as a fundamental process of HHG, is highly sensitive to the waveform of driving pulses due to its exponential dependence on the laser intensity [20]. By superposing a weak control field at another wavelength onto an

intense laser field, the waveform of the driving field will be tailored on sub-cycle time scale. The broken symmetry of the laser field enlarges the difference of ionization rate as well as HHG yield between the adjacent half optical periods. Therefore, a shaped laser pulse allows for sub-cycle manipulation of HHG, leading to the enhancement of XUV emission in some half cycles and the weakening of XUV emission in some other half cycles.

In the next two processes (i.e., propagation and recombination) of HHG, the waveform of driving pulses determines the electron trajectory, the excursion time in the laser field and the kinetic energy obtained from the laser field. Therefore, by using a waveform-controlled laser field, we can extend cutoff energy of HHG, broaden and tune the spectrum of XUV supercontinuum, and select quantum trajectories. To give a clear view, we depict schematic diagrams of HHG in one-color and two-color laser fields, as shown in Figs. 1(a) and (b) respectively. In Fig. 1(a), there are three electron trajectories contributing to HHG, originated from the electrons ionized at the time 1, time 2, and time 3. Because the central half cycle of the optical pulse is much more intense than any other half cycles, the electron ionized at time 2 will gain more energy upon the recollision than all the electrons ionized at the other times. Hence, we will obtain an attosecond pulse train, with the pulse 2 having the highest photon energies. Then, we can place a metal foil to block all these two-pulses composed of the low-energy photons, only part of the pulse 2 is allowed to pass through due to the higher photon energies it carries. In the spectral domain, it corresponds to an XUV supercontinuum spectrum. Therefore, in order to obtain IAPs, we need to have a few-cycle driving pulse with an intense central half cycle, but relatively weak neighboring half-cycles. The contrast between the central half cycle and the neighboring cycles will determine the bandwidth of supercontinuum emission and the pulse duration of attosecond pulses.

Fortunately, the synthesis of two-color fields provides us an effective method to enhance the contrast between the central half cycle and the neighboring half cycles. As shown in Fig. 1(b), if we add a second harmonic wave upon the fundamental wave, we can effectively enhance the central peak, and suppress these two neighboring peaks, which is equivalent to shortening of pulse duration. In this case, we can obtain broader supercontinuum spectra and shorter attosecond pulses due to the modified electron trajectories (See red dashed line in Fig. 1(b)).

III. ADVANTAGES OF HHG IN A TWO-COLOR LASER FIELD

III-1. The broadening of XUV supercontinuum and generation of IAP

Generally, HHG inherently produces attosecond pulse trains separated by about half optical period of the driving laser field. Therefore, to achieve IAPs desired for a lot of applications, it is necessary to gate the driving pulses or the harmonic emission itself, making the HHG process periodically occurring in a multi-cycle regime can be virtually reduced to only once. By gating the driving field with CEP-stabilized, few-cycle laser pulses, one has broken through the 100-as barrier [21]. However, up to now, the achievement of few-cycle, high-energy laser pulses is still a challenge for most laboratories, which hampers the widespread use of attosecond technology. The commercial availability of multi-cycle, high-energy laser

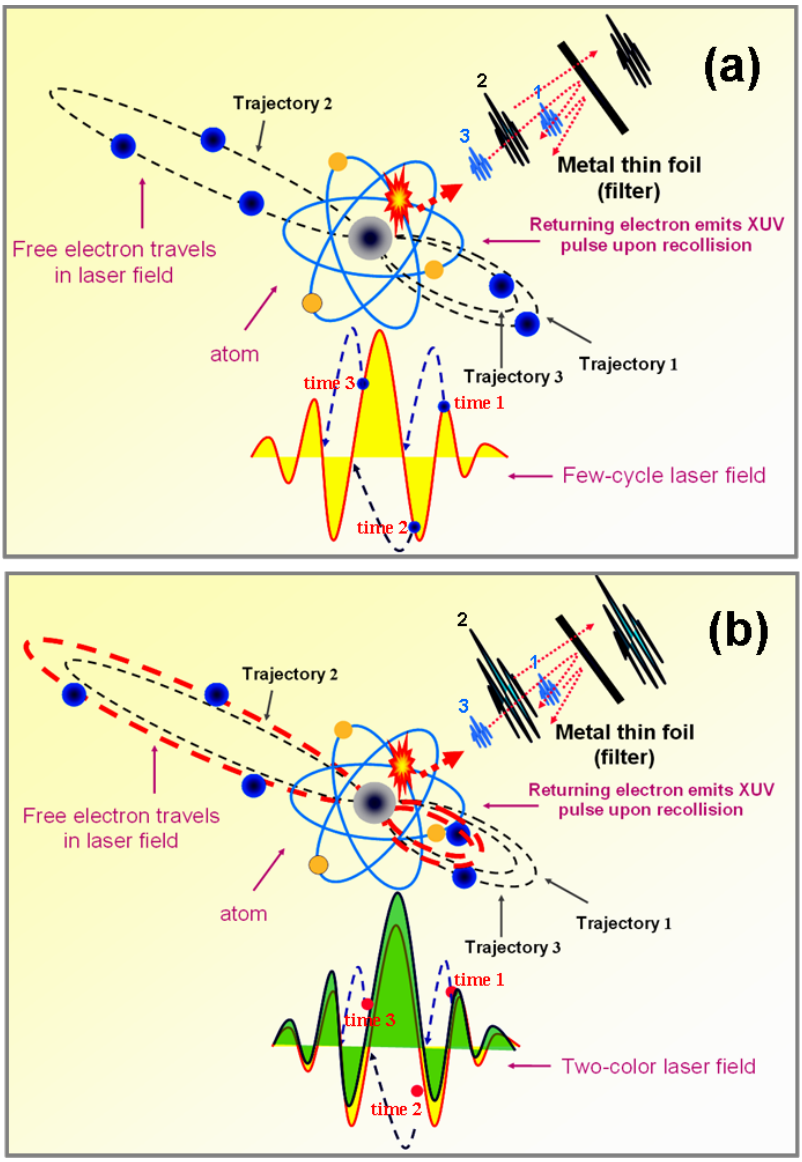

FIG. 1: Schematic diagrams of HHG in (a) one-color and (b) two-color laser fields.

system motivates us to explore other methods, such as multi-color field synthesis [17, 22], polarization gating [23], double optical gating (DOG) [24], phase matching gating [25], etc., which are capable to gate HHG itself on a sub-cycle time scale. In this review, we focus on the two-color field scheme. As compared to one-color laser field, the two-color synthesized field provides us more parameters (e.g., wavelength ratio, intensity ratio, time delay, relative angle of polarization planes, etc.) to control electron wavepackets, leading to high flexibility of experimental implement. In this section, we will show the capability

of two-color field for broadening XUV supercontinuum and shortening attosecond pulses.

A. Parallel-polarized two-color field scheme

The parallel-polarized two-color field is a common and simple waveform shaping method. In the scheme, the main field and the control field have the same polarization direction, and thus the polarization of their synthetic field is time independent, which means the electron travels along a one-dimensional (1D) path. However, taking advantage of the simple technique, we can significantly extend XUV supercontiuum spectrum and break through the bottleneck of 100 as due to the high sensitivity of HHG on the laser waveform [19]. Figure 2(a) shows electric fields of the 6-fs, 800-nm pulse (dashed line), the two-color pulses composed of 800-nm and 400-nm pulses at zero delay (dashed dotted line), and at the time delay of -166.7 as (solid line). In our simulation, the single-atom response of HHG is calculated using the Lewenstein model [26, 27] based on a single-active-electron approximation. It should be pointed out that all simulated spectra shown in the review are obtained by the method. The calculated HHG spectra in the three driving fields are shown in Fig. 2(b). Clearly, the minor difference of the three laser fields leads to the dramatic change of HHG spectra. The XUV supercontinuum spectrum produced by the single 6-fs pulse alone shows a bandwidth of approximate 30 eV. In this case, although a single attosecond pulse is generated, its temporal profile shows two subpulses with comparable peak intensities, and each subpulse is longer than 100 as, as shown by curve III of Fig. 2(c). A significantly broadened XUV supercontinuum with a spectral width of ~ 75 eV can be achieved by superposing the weak frequency-doubled pulse onto the fundamental pulse with a zero time delay. Surprisingly, XUV supercontinuum is dramatically broadened to 148 eV when we introduced a relative phase shift of $t_0 = -166.7$-as between two-color pulses. The ultra-broad XUV supercontinuum can support an isolated 65-as pulse even without any phase compensation, as shown by curve II of Fig. 2(c). Furthermore, if all the phase dispersion over the spectral width of 148 eV can be properly compensated for, an isolated 23-as pulse with a clean temporal profile could be theoretically predicted [See curve I of Fig. 2(c)]. Therefore, parallel-polarized two-color field with the optimized delay offers an effective method to obtain extremely broad XUV superconituum as well as IAPs close to an atomic unit under the conditions available in quite a few laboratories around the world. This surprising result gave us a lesson that the electron motion is very sensitive to the waveform of light field.

Additionally, with the method, it has been experimentally demonstrated the generation of the XUV supercontinuum in argon with a two-color laser field consisting of an intense 7-fs, 800-nm pulse and a relatively weak 37-fs, 400-nm pulse [28]. By controlling the relative time delay between the two laser pulses, one has observed both enhanced HHG and spectral broadening of the supercontinuum.

B. Orthogonal-polarized two-color field scheme

Furthermore, we extended this technique into the orthogonal-polarized two-color laser field. As compared to parallel-polarized two-color field, the driving pulse composed of orthogonal-polarized two-color field has a rapid varying polarization on sub-cycle time scale, and thus it can effectively control electron wavepacket (e.g., its traveling path, the recolliding direction, etc.) in two-dimensional (2D) space. Actually, the orthogonal-polarized

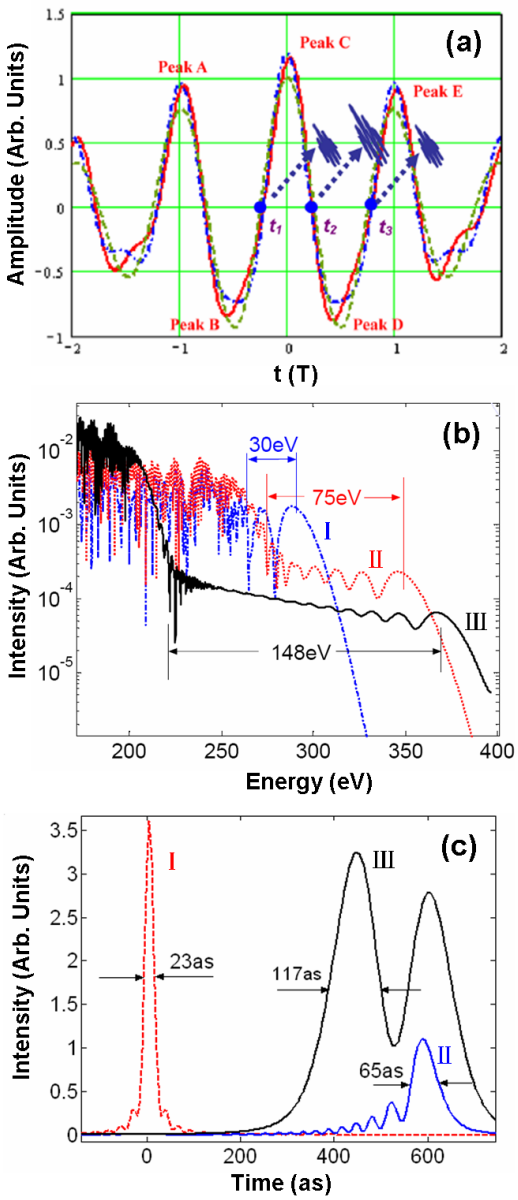

FIG. 2: (a) Electric fields of the single 6-fs pulse (dashed line), the two-color pulses without a time delay (dashed dotted line), and with a −166.7-as time delay (solid line). (b) The spectra of the XUV supercontinua generated with the single 6-fs pulse (dashed dotted line), the two-color pulses without a time delay (dotted line), and with a −166.7-as time delay (solid line). (c) The temporal profiles of the attosecond pulses generated from the XUV supercontinuum of 148 eV spectral width with (red dashed line) and without (blue solid line) phase compensation. For comparison, the attosecond pulse generated by the single-color 6 fs pulse without phase compensation is shown as black solid line.

two-color field scheme can be recognized as a combined version of parallel-polarized two-color field technique and polarization gating technique. Therefore, in principle, it should be easier to broaden XUV supercontinuum emission as compared to the parallel-polarized two-color field.

As an example, we theoretically demonstrated the generation of XUV supercontinuum in an orthogonally polarized two-color laser field synthesized by two sinusoidal pulses at 800-nm and 1300-nm wavelengths, both with a pulse duration of 9-fs and an equal peak intensity [29]. As shown in Fig. 3(a), the synthesized electric field shows an asymmetric, rapidly varying waveform and polarization in three-dimensional (3D) space. In the case, the electron born at certain moments can be driven back to its parent ion after traveling along a curved trajectory in a plane perpendicular to the beam propagation direction, while the electron at some moments can never revisit the parent ion and thus it does not make any contribution to HHG. The x and y components of HHG spectra generated by the driving field are shown in Fig. 3(b). In order to give a clear view, we purposefully shift the y component of the HHG spectrum to lower location. The x component of the HHG spectrum [the upper curve in Fig. 3(b)] shows a smooth XUV supercontinuum covering almost the entire plateau region. In contrast, in the lower curve in Fig. 3(b), significant spectral modulation appears in the low energy range, indicating the existence of multiple electron recolliding events capable of contributing to the generation of low-order high harmonics polarized in the y direction. The spectral modulation originates from the interference between the low-order harmonics emitted at different times. By performing inverse Fourier transformations of the XUV supercontinuum from 25 eV to 325 eV, we obtained the electric fields of the attosecond pulses in 3D space and their corresponding temporal envelopes, as shown in Figs. 3(c) and (d), respectively. Clearly, the supercontinuum in the spectral range can synthesize an attosecond pulse train and each attosecond pulse in the pulse train shows different polarization states, which is determined by the moving direction of the electron at the moment of recombination. The unique property opens up a new avenue to control the polarization of attosecond pulses using the orthogonal-polarized two-color field [30]. On the other hand, it can trigger a series of interesting phenomena in molecular HHG, where the conversion efficiency of HHG critically depends on the angle between the laser polarization direction and the molecular axis [31]. In other words, the sensitivity of the molecular HHG to the angle between the moving direction of the recolliding electron and the molecular axis provides an additional way to further confine the temporal window of HHG and eliminate undesirable satellite attosecond pulses shown in Figs. 3(c) and (d).

Based on the above consideration, we employed the technique of the orthogonal-polarized two-color field to molecular HHG [32]. Figure 4(a) shows HHG spectra of argon (Ar) generated by the driving field consisting of a 9-fs, 800-nm, x-polarized pulse and a 15-fs, 1300-nm, y-polarized pulse. Obviously, both the x and the y components of the HHG spectrum of Ar show smooth XUV supercontinua in the spectral range of 80–100 eV. However, in the low-energy range, especially in the y component, there is a significant spectral modulation originating from the interference between the attosecond pulses emitted at different times. This property can be seen more clearly from the temporal profiles of the high harmonics in the spectral range of 50–100 eV, as shown in Fig. 4(b). We noted

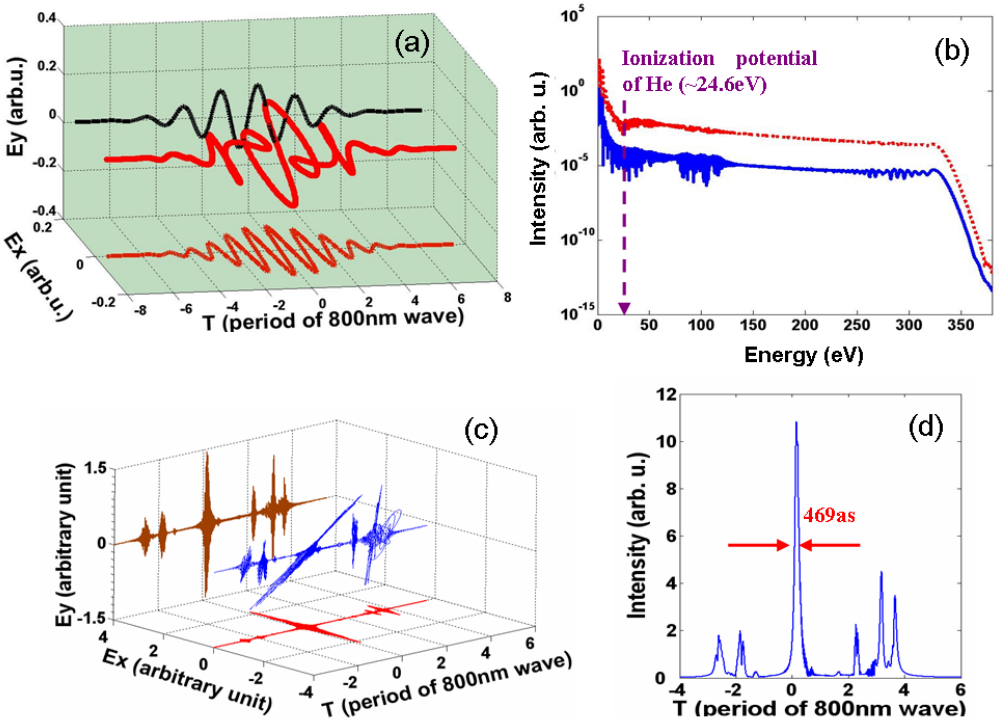

FIG. 3: (a) 3D plot of the orthogonally polarized two-color laser field; (b) x and y components of the high-order harmonic spectrum produced in the orthogonal-polarized two-color field; (c) 3D plots of electric fields of attosecond pulses generated by Fourier syntheses of the harmonics in the spectral ranges of 25–325 eV and (d) corresponding pulse envelope.

that the pulse train contains two single attosecond pulses, namely, a main pulse released at about $0.3T$ and a weak one at $\sim 2.5T$, where T is the period of an 800 nm pulse. In addition, it was also found that the polarization directions of the two pulses were different, implying that the electrons return to the vicinity of cores with varying incident angles due to the change of the polarization direction of the synthesized field with the time. The main pulse polarizes along the direction of $\sim 45°$ with respect to x axis, while the satellite pulse polarizes along the y direction. When the interaction medium is switched to molecular nitrogen (N_2) from Ar, the case will be different. Figures 4(c) and (d) show HHG spectra of N_2 with the molecular axis oriented at 45° with respect to x direction and the attosecond pulses synthesized by harmonics in the same spectral range, respectively. Comparing to the HHG in Ar, both x and y components of HHG spectra in N_2 become smoother in the low-order harmonics and the weak satellite pulse generated at $\sim 2.5T$ disappears. The reason is that, when the molecular axis is along the moving direction of the recolliding electron (i.e., the polarization direction of the main attosecond pulse), the electron ionized from the

highest occupied molecular orbital (HOMO) of N_2 has the highest probability to recombine with its parent ion [33]. In this case, the efficiency of HHG corresponding to the main attosecond pulse reaches its maximum, while the efficiency of HHG corresponding to the y-polarized satellite pulse is effectively reduced. In this way, the undesirable satellite pulse is eliminated. Therefore, by means of the sensitivity of HHG on the molecular orientation, the rapid variation of moving direction of the recolliding electron in the orthogonal-polarized two-color laser field can be employed for further confining the temporal window of HHG and isolating single attosecond pulse from attosecond pulse train.

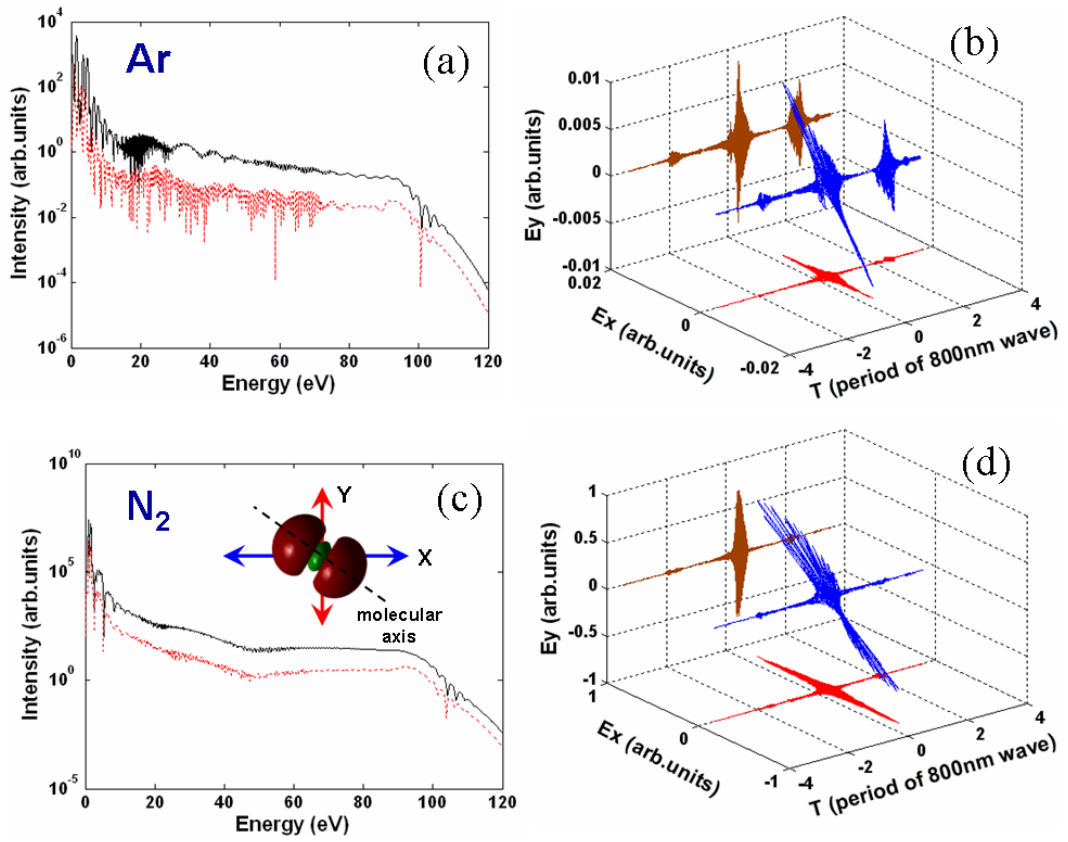

FIG. 4: x (solid line) and y (dotted line) components of high-order harmonic spectra from (a) Ar and (c) N_2 aligned at 45° with respect to x axis in the orthogonal-poalrized two-color field; (b) and (d) are the corresponding electric fields of attosecond pulses synthesized by the harmonics in spectral range of 50–100 eV.

C. Broad supercontinuum generation in multi-cycle laser fields

Although both parallel- and orthogonal-polarized two-color field schemes can dramatically extend the bandwidth of XUV supercontinuum spectra, they usually require at least one ultrashort pulse with the pulse duration of 1-2 optical cycles in order to create sub-100as IAPs. The energy loss caused by the pulse compression largely reduces the output energy of IAPs. Therefore, considerable effort has been devoted to generating IAPs

with multi-cycle pulses directly from the chirped pulse amplifier. Currently, several methods have been proposed for broadening XUV supercontinua in the long pulse regime, e.g., DOG [24], generalized double optical gating (GDOG) [34], adding a nonlinear chirp on the multi-cycle driving field [35], etc.

We found a simple method to generate sub-100as IAPs by use of a multi-cycle two-color laser field [22]. Theoretical simulation demonstrated that the supercontinuum spectrum was significantly broadened by optimizing the time delay and the angle of polarization planes between two multi-cycle, linear-polarized laser fields. In Fig. 5(b), we can clearly see an extremely broad XUV supercontinuum with the bandwidth of 180 eV when the polarization between an intense 800-nm, 25-fs laser pulse and a relatively weak 1400-nm, 43-fs laser pulse is arranged at an angle of ~ 73 degree and the time delay is adjusted at 3.63 fs. In contrast, in the case with either 800-nm or 1400-nm one-color field, no observable supercontinuum is generated in the multi-cycle regime. Figure 5(a) illustrates the driving field consisting of 800-nm and 1400-nm pulses. The x component of synthesized field is a one-color field at 800 nm, while the y component is a two-color field composed of 800 nm and 1400 nm laser pulses and exhibits a high asymmetry. Due to this reason, polarization state of the synthesized field rapidly changes within an optical period, which allows us to purposely manipulate the free electron trajectories contributing to HHG. Furthermore, the ultra-broad supercontinuum generated by the synthesized field can support a ~ 73-as IAP even without any phase compensation when the long trajectory is removed, as shown in Fig. 5(c). The ability of the two-color field scheme to generate sub-100as IAPs in the multi-cycle regime relaxes the requirement of attosecond pulse generation for pulse duration of laser system and avoids the energy loss of the pump pulse caused by a complex compressing device. Consequently, it holds great potential for generation of stronger and shorter IAPs in the future.

More interestingly, we experimentally generated EUV supercontinuum with a high-energy, multi-cycle, one-color laser field [36]. The experimental setup is sketched in Fig. 6(a). The 11-mJ, 35-fs, 800-nm laser pulses directly from the laser system (Legend Elite Cryo PA, Coherent Int.) are focused by $f = 100$ cm lens into 30-mbar Krypton. HHG spectra are detected by home-made X-ray grating spectrometer equipped with a X-ray CCD (Princeton Instruments, 1340×400 imaging array PI:SX 400). A long filament channel can be clearly seen at the both sides of the gas cell, as shown in inset of Fig. 6(a). It is noteworthy that although our gas cell is only 10-mm-long, there are two holes drilled by the driver laser pulses at the two ends of the cell through which leakage of krypton gas inevitably occurs. Actually, the leaking gas from the holes could form a favourable density distribution of the krypton gas outside the gas cell for inducing filamentation and self-compression of the driver pulses. By performing a SHG-FROG measurement, we retrieved the temporal intensity and phase of the driving pulse coming out from gas cell, as illustrated in Fig. 6(b). Apparently, the driving pulses are split into several intensity spikes at the end of the filament due to propagation effects. In fact, at different interaction lengths, the waveform of the driving pulses could be different. Both the pulse shaping naturally occurring in the interaction region and propagation effects involved in HHG lead to EUV supercontinuum generation in the high-energy, multi-cycle, one-color laser field. Figure 6(c) shows a typical

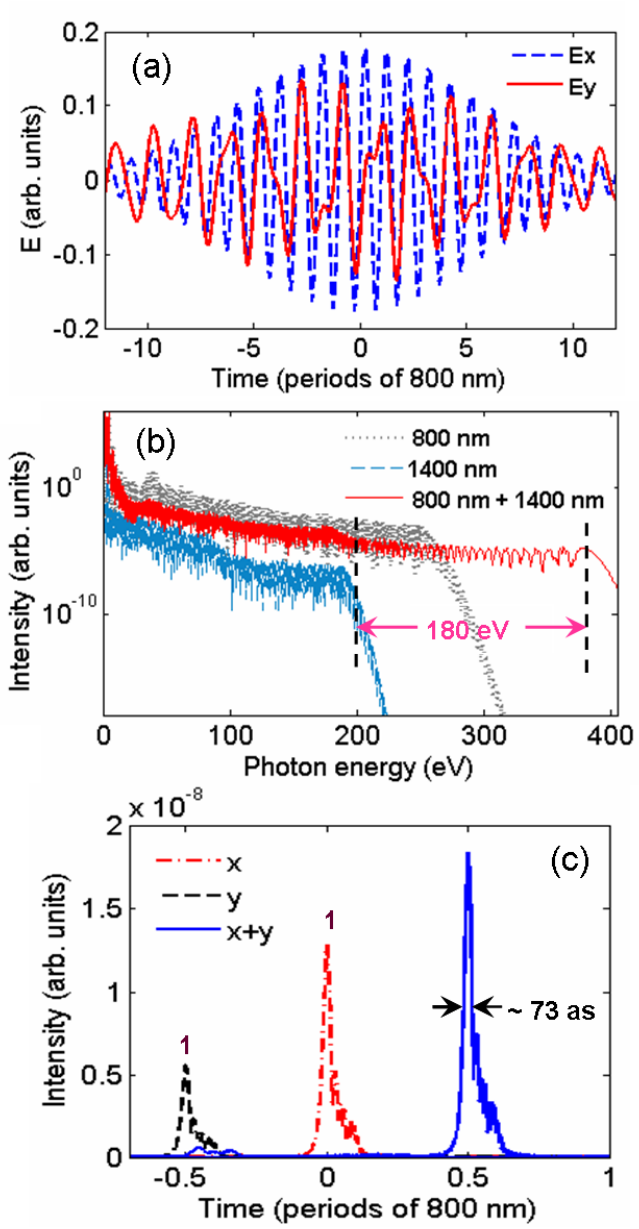

FIG. 5: (a) x and y components of the synthesized laser field; (b) Harmonic spectra generated with the 800-nm laser field (dotted curve), 1400-nm laser field (dashed curve), and their synthesized field (solid curve); (c) Envelope of attosecond pulses obtained by performing inverse Fourier transformation for the supercontinuum from 200 eV to 380 eV after removal of the long trajectory.

single-shot HHG spectrum with photon energies spanning from 35 eV to 50 eV, which can support a $\sim$ 270-as IAP by assuming a flat phase. This new technique greatly simplifies the experimental setup of attosecond pulse generation and efficiently utilizes the driving pulses, so it is a promising way for generating intense attosecond pulses. These advantages will have important implementations for attosecond science and technology.

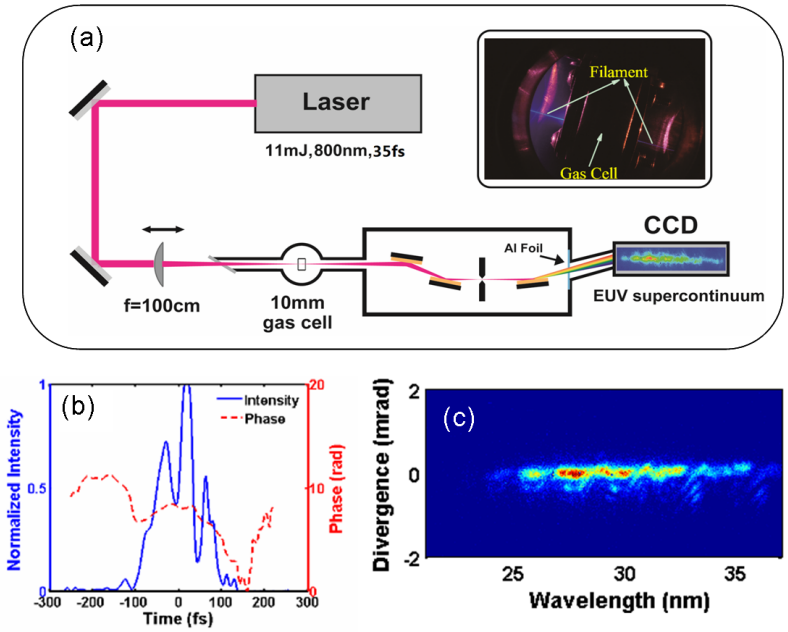

FIG. 6: (a) Schematic of the experimental setup; (b) Retrieved temporal intensity (solid line) and phase (dashed line) of driving pulses coming out from gas cell; (c) Single-shot supercontinuum spectrum generated by $\sim$ 35-fs, 11-mJ laser pulses.

III-2. The selection of single quantum trajectory

The employment of two-color field can create spectrally smooth XUV supercontinua by selecting long or short quantum trajectory in HHG, leading to clean temporal profiles of IAPs. When a 64-fs, 2400-nm control pulse is superposed onto a 6-fs, 800-nm main pulse, the short quantum trajectory is selected while HHG from long trajectory is effectively suppressed [37]. In order to give a clear view, Figs. 7(a) and (b) indicate the classical analysis and time-frequency analysis for HHG driven by the two-color field above. Figure 7(a) shows the synthesized electric field (dashed line), the electron return kinetic energy (solid line) as a function of time calculated by classical three-step model [1], and the tunnel ionization rate calculated by Ammosov-Delone-Krainov (ADK) model (gray filled curve) [20]. Obviously, one can see that the electrons tunnel-ionized around time $t_{\max}$ will recombine with the ions with the highest return energies. A remarkable feature shown in Fig. 7(a) is that, almost all of the electrons tunnel-ionized around the time $t_{\max}$ are actually freed from a binding state at those moments on the "short trajectory" side. This implies that the major contribution

of HHG is from the short quantum trajectory. The corresponding time-frequency analysis shown in Fig. 7(b) provides further evidence for the selection of short trajectory in the two-color field.

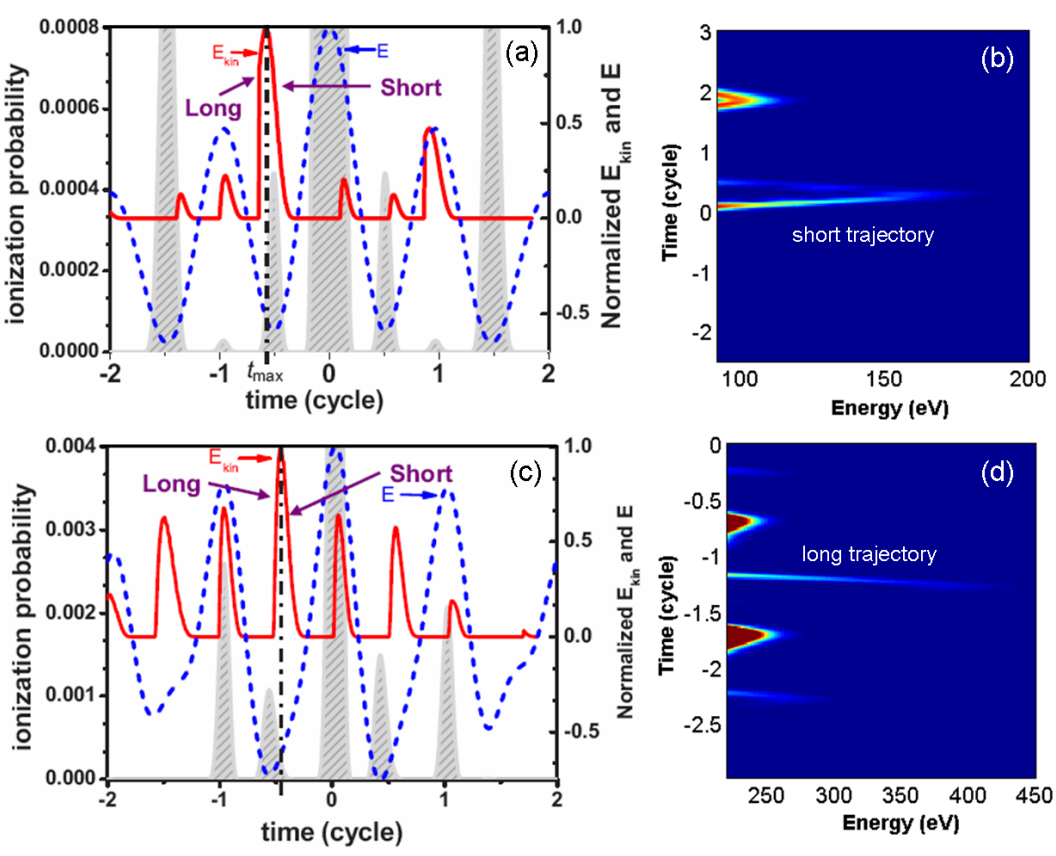

FIG. 7: Normalized electron kinetic energy (solid line), electric field (dashed line), and the ionization probability (gray filled curve) as a function of time in the driving field synthesized by (a) 800-nm and 2400-nm laser pulses and (c) 800-nm and 400-nm laser pulses, respectively. (b) and (d) are the corresponding time-frequency analyses for HHG in two synthesized fields.

We also found that not only the short trajectory but also the long trajectory can be selected using the two-color field schemes [19]. When a two-color laser field synthesized by a 6-fs, 800-nm main pulse and a 21.3-fs, 400-nm control pulse with the time delay of −166.7 as is employed for HHG, the dominant quantum trajectory contributing to HHG will be switched to the long trajectory from the short trajectory. Its direct evidence can be obtained with the classical calculation and time-frequency analysis, as shown in Figs. 7(c) and (d), respectively. In Fig. 7(c), we can clearly see that most of the ionized electrons that could contribute to the XUV supercontinuum generation actually travel along the long trajectory before they recombine with their parent ions. This reveals the mechanism of the formation of the smooth spectral profile of the ultra-broad XUV supercontinuum we

observed in Fig. 2(b) (curve III).

III-3. The generation of narrow-bandwidth, wavelength-tunable XUV emission

Typically, high-order harmonic emission consists of a few rapidly decreasing harmonics followed by a plateau with a sharp cutoff, so that HHG spectrum always covers a broad spectral range with comparable intensity due to its nonperturbative nature. However, wavelength-tunable XUV radiation with a narrow spectral bandwidth is of potential importance in many fields such as the resonant excitation of atoms and molecules by XUV pulses, the seeding of XUV or X-ray free electron laser, and so on. In order to create this kind of coherent light source via HHG, a series of methods have been explored. The most straightforward method is to use a filter, grating or monochromator to spectrally select the desirable spectral components of the input beam [38–40]. However, these optical elements usually induce extra loss in the XUV regime. Another approach to obtain narrow-bandwidth XUV radiation from HHG is to precisely control the phase matching by carefully tailoring the shape of driver pulses in a feedback system [41] or by performing quasi-phase-matching technique [42]. However, these methods based on phase matching are usually complex and difficult to implement. Fortunately, HHG driven by a two-color laser field shows great potential to select and control high-order harmonic spectrum, allowing for direct generation of narrow-bandwidth, tunable XUV emission in HHG by two ways as follows. This will be discussed in detail in the section.

One strategy is to selectively enhance single or several harmonic orders by manipulating the electron wavepacket with the two-color field. We theoretically demonstrated the selective enhancement of HHG in two-color laser fields consisting of a 3-fs, 800-nm laser pulse with a laser intensity of 3×10^{14} W/cm^2 and a 64-fs, 400-nm laser pulse with a laser intensity of 1×10^{14} W/cm^2 [43]. Figure 8(a) shows HHG spectra calculated at time delay of 0.75 fs, 1 fs, 1.25 fs, 1.5 fs, 1.75 fs and 2 fs. Interestingly, although these HHG spectra show nearly the same cutoff energies at $\sim$ 200 eV, a phenomenal enhancement of the XUV radiation with a bandwidth ranging from 3 eV to 10 eV can be observed at different positions of each HHG spectrum. For each time delay used in our simulation, the enhancement factor is almost one order of magnitude. The central frequency of the enhanced XUV radiation can be continuously shifted from the beginning of HHG plateau to the cutoff region by scanning the time delay, leading to a wide tuning range spanning from $\sim$ 50 eV to $\sim$ 150 eV. Furthermore, the selectively enhanced HHG gave rise to a bandwidth-controllable XUV supercontinuum in the plateau region, facilitating generation of intense isolated attosecond pulses. Further investigation revealed this enhancement effect is a result of the modified electron trajectories in the complex optical waveform offered by the two-color laser field. Figure 8(b) illustrates the electric field of the two-color laser pulse with the 1.5-fs time delay (dashed curve), the electron return energy as a function of its ionization time calculated by the classical three-step model (solid curve) [1] and the ionization probability (grey filled curve) calculated by the ADK model [20]. Obviously, the waveform of the two-color laser field fundamentally deviates from that of a single-color laser field, particularly evidenced by the two pits A and B presented in the two-color laser field. The electric field approaches zero near these two pits. Because of these two pits, the electron return energy curve as a

function of time (solid curve) in Fig. 8(b) also shows two pit-like structures, as indicated as the pits C and D. Since the tunnel ionization is a highly nonlinear optical process which is very sensitive to the strength of the electric field, the strongest ionization of the Ar atom occurs at a time corresponding to the maximum peak electric field. Therefore, most of the ionized electrons which contribute to selectively enhanced XUV radiation will travel along the folded electron trajectory with the pit C. On the other hand, the folded region of electron trajectory corresponds to the comparable return kinetic energy, and thus the constructive interference between XUV radiation from the folded trajectory leads to the selective enhancement of HHG.

Although the two-color field scheme above provides a simple, all-optical approach for finely control of HHG spectra (i.e., central wavelength and bandwidth), it requires the nearly single-cycle laser field. In order to relax the experimental requirement, we further investigated narrow-bandwidth, tunable HHG in a three-color laser field [44]. The enhancement of HHG in a selected spectral range was observed due to the modified electron trajectory in the shaped laser field consisting of a 5-fs, 800-nm pulse, a 15-fs, 2000-nm pulse and a 25-fs, 2200-nm pulse. Particularly, recently the selective enhancement of a single harmonic has been experimentally demonstrated by using a three-color laser field synthesized by the 800-nm main pulse and two control pulses at 400 nm and 267 nm with perpendicular polarizations [45].

The other strategy is to confine HHG occurring in a narrow spectral range. The trick of the technique is that only the electron born at a specific time can come back and recombine with the ion, contributing to HHG. For these electrons, they carried a fix amount of kinetic energy so that they can only release photons with a fixed energy upon recollision. In this way, we can create narrow-bandwidth HHG spectra with a high contrast (i.e., the ratio between the selected harmonics and the adjacent harmonics). Theoretical investigation demonstrated that an orthogonal-polarized two-color laser field has the ability to gating HHG in spectral domain [46, 47]. In our simulation [46], the driving field is synthesized by an intense 10-fs, 1500-nm pulse polarized in x direction and a relatively weak 40-fs, 2400-nm pulse polarized in y direction. When the intensity of 1500-nm laser pulse is 6×10^{14} W/cm^2, and the amplitude ratio A and time delay between the 2400-nm and 1500-nm laser pulses are set to be 0.5 and ~ 2.17 fs, respectively, the evolution of the synthesized electric field in 3D space is shown by green curve in Fig. 9(a). Clearly, in the superposing region of the two laser fields, the polarization state of laser field exhibits a rapid and complex variation within an optical cycle. Surprisingly, both x- and y-components of harmonic spectra show a peak around 270 eV, as shown in Fig. 9(b). In this way, XUV radiation with a bandwidth of ~ 4 eV is well selected from the broad plateau region of the HHG spectrum. The selected harmonics are about two orders of magnitude stronger than the adjacent harmonics. To give a clear demonstration, the harmonic spectra polarized in both x and y directions are shown in linear scale (see inset of Fig. 9(b)). We can clearly see that in the y direction, the spectrum of the selected XUV radiation shows a smooth profile, which allows us to synthesize isolated pulses with the sub-cycle duration. However, the XUV radiation in the x direction, which has broad spectrum with deep modulations, is more than one order of magnitude weaker than that in the y direction. Furthermore, we

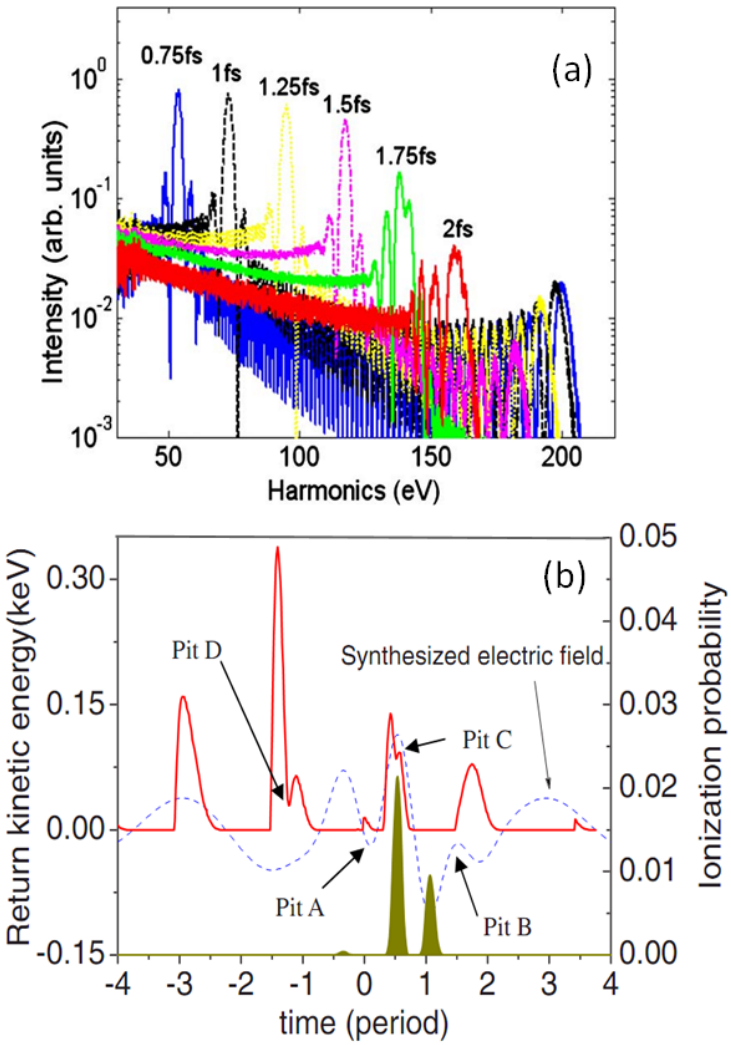

FIG. 8: (a) High-order harmonic spectra generated by the synthesized field consisting of a 3-fs, 800-nm pulse and a 2400-nm pulse at different time delays; (b) The synthesized laser field (dashed curve), the electron return energy (solid curve) and the ionization probability (gray filled curve) as a function of the time.

found that the central wavelength of the narrow-bandwidth XUV emission can be tuned in an extremely broad range by adjusting the laser intensity of 1500-nm pulses or the amplitude ratio A of two laser fields, as shown in Figs. 9(c) and (d), respectively.

Why is HHG confined within a narrow spectral range? In order to gain the insight into the physics underlying the narrow-bandwidth HHG, we perform classical analysis based on the three-step model of HHG [1]. Figure 10(a) shows the minimum returning distance of electron (blue solid curve) and its returning kinetic energy (red dashed curve) as a function

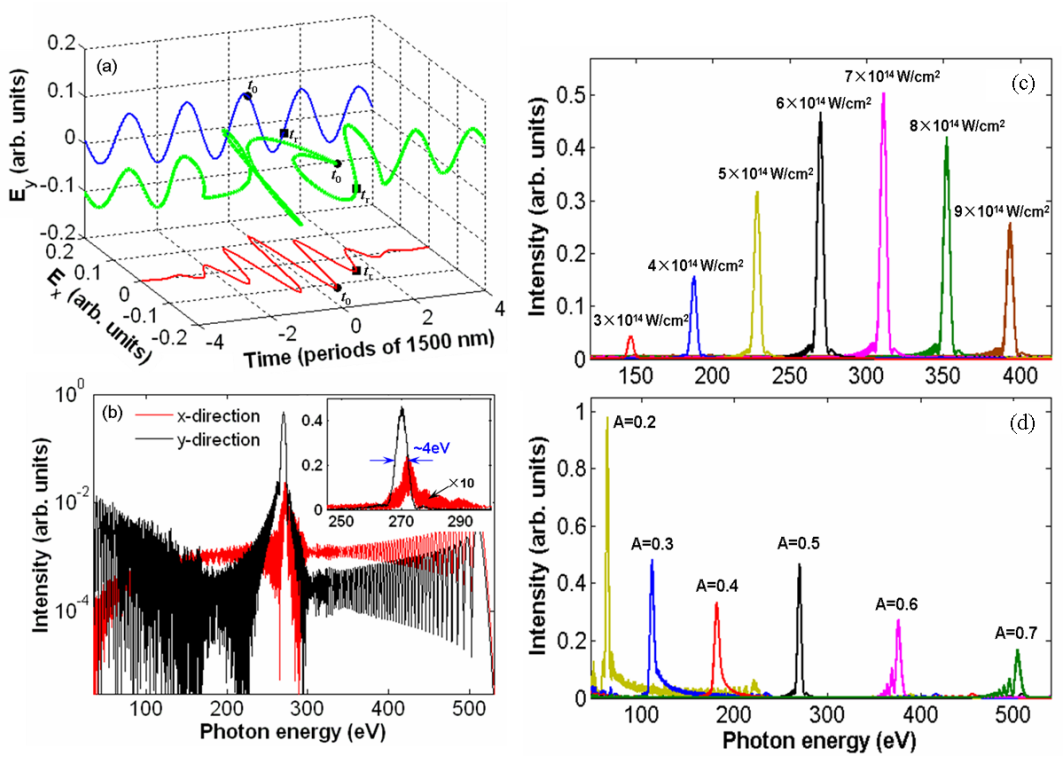

FIG. 9: (a) 3D plot of the driving field synthesized by a 1500-nm, 10-fs laser field polarized in the x direction and a 2400-nm, 40-fs laser field polarized in the y direction. The amplitude ratio (A) and time delay between the two laser fields are 0.5 and $\sim$ 2.17 fs, respectively. (b) The x (red curve) and y components (black curve) of high-order harmonic spectra generated by the synthesized field in (a). Inset: High-order harmonic spectra in a linear scale. High-order harmonic spectra obtained (c) at different intensities of 1500-nm pulses and (d) at different amplitude ratios (A = 0.2–0.7) between 2400-nm and 1500-nm pulses.

of birth time (i.e., the time at which the electron is tunnel ionized). It can be seen that only the electron born at t_0 (indicated by a red dot) can accurately return to its parent ion (i.e., its displacement from ion approaches zero) , while electron born before or after t_0 has a rapidly increasing displacement. When the displacement is so large that electron cannot recombine with parent ion, HHG will terminate. The dominant contribution to HHG comes from the electrons born within a small temporal window centered at t_0, as indicated by the rectangle (shaft-gradient color filled) in Fig. 10(a), and these electrons obtained almost the same kinetic energy in the laser field, leading to narrow-bandwidth XUV emission. For better understanding the electron motion in the specific laser field, in the Figs. 10(b)–(d), we depict 2D classical trajectories for the electrons born at t_0-50as, t_0, and t_0+50as, respectively. The electron born at t_0 comes back to its initial position (the initial position is indicated by the red solid dot) at t_r along a curved trajectory [see Fig. 10(c)] and then a high energy photon can be generated when the electron is captured by the parent ion. We

also notice that the recolliding electron moves in a direction nearly parallel to the y-axis, as indicated by the red arrow in Fig. 10(c). Accordingly, the birth time (t_0) and the return time (t_r) of the electron are indicated by the black dots and black squares in Fig. 9(a), respectively. As shown in Fig. 9(a), since the recolliding electron is born near the peak of the electric field, and then recombines with its parent ion when the strength of electric field is near zero, the polarization direction of high-order harmonic emission can be considered to be the same as the moving direction of the recolliding electron (i.e., the high-order harmonic emission from the trajectory is polarized almost along the y-axis). When the electron is ionized 50 as before or after t_0, the minimum distances between the return electrons and its parent ion reach up to ~ 50 atomic units (a.u.), as illustrated in Figs. 10(b) and (d), respectively. Therefore, in these two cases, harmonic emission will significantly decrease or even terminate because of a great drop in recombination probability. The classical analysis above clearly reveals that the constructed laser field realizes the attosecond control of electron dynamics. In this way, only the electron from a single trajectory can come back with a fixed kinetic energy and recombine with the ion so that HHG only efficiently occurs in a narrow spectral range.

Furthermore, we extended the technique to molecular HHG [47]. It was found that the peak intensity of narrow-bandwidth XUV emission strongly depends on molecular alignment angles. Therefore, this technique not only has important applications in XUV nonlinear optics, but also may provide us an alternative method for extracting the structural information of molecular orbitals.

III-4. The enhancement of HHG yield

The low yield of HHG largely limits its widespread use in many fields. Therefore, considerable effort has been devoted to developing efficient harmonic conversion techniques. By loosely focusing a high-energy laser pulse into a long gas cell or gas jet, HHG in the absorption-limited regime has been obtained under the optimized phase matching condition [48, 49]. In order to further enhance HHG yield, one also proposed some new techniques, such as the synthesis of two-color field [28, 50, 51], quasi-phase matching [42], mixture of two gases with different ionization potentials [52, 53] and preparation of excited state atom [54]. In the review, we mainly focus on two-color field scheme. It has been experimentally demonstrated that the employment of both parallel-polarized and orthogonal-polarized two-color field can effectively enhance HHG yield [28, 50, 51]. Particularly, by applying a second harmonic with a high intensity, high-order harmonics are more than two orders of magnitude stronger in the orthogonal-polarized regime as compared to one-color field [50]. Very recently, it was demonstrated that the generation of intense isolated attosecond pulses with the energy up to 1.3 μJ by combing a two-color field scheme and an energy-scaling method of HHG [51].

However, as mentioned in section II, the trick of the two-color field technique to dramatically extend supercontiuum spectra is to enhance the intensity contrast between the central half cycle and the neighboring half cycles. In this way, HHG yield corresponding to the supercontinuum is usually significantly lower than that produced by the one-color driving field because of the relatively low ionization rate for those electrons of the highest

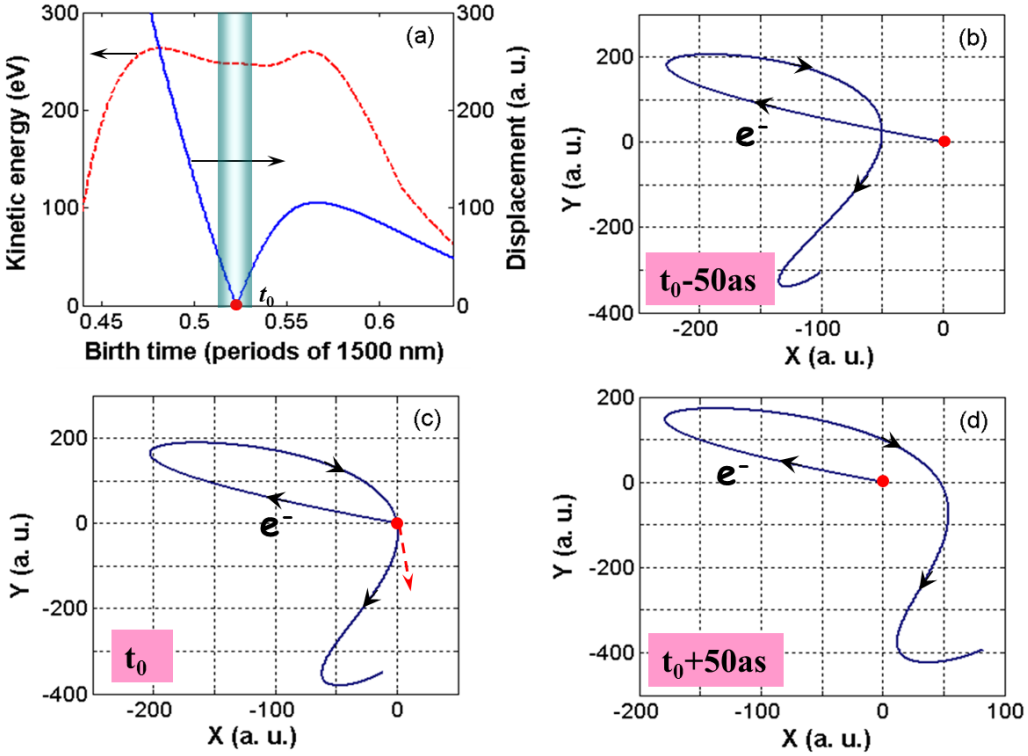

FIG. 10: (a) Return kinetic energy (red dashed curve) and minimum returning distance of electron (blue solid curve) as a function of birth time; 2D classical trajectories for electrons born at the times (b) t_0-50as, (c) t_0, and (d) t_0+50as. Initial positions of the electron are indicated by red solid dots, and the moving direction of the recolliding electron is indicted by the red arrow in (c).

kinetic energy upon recombination [19, 22]. In order to address the problem, we replaced the cosine-waveform by a sine-waveform counterpart in order to create a better waveform of two-color laser field by which both supercontinuum emission and IAPs were significantly enhanced [55]. It is well-known that when a sine-waveform few-cycle pulse is used, then two attosecond pulses will be generated in the laser field. In this case, because these two pulses have comparable photon energies, spectral filtering cannot be applied for selecting out an isolated attosecond pulse. However, one may recognize that these two attosecond pulses generated by the sine-waveform few-cycle field will have different intensities because of the different tunnel ionization ratios within different half cycles. Moreover, the shorter the duration of the few-cycle driving pulse with a sine-waveform, the greater the difference between the ionization ratios of the recombination electrons giving rise to the two attosecond pulses, and consequently, the intensities of the two attosecond pulses themselves. This is why in the experiment of generating $\sim$ 80-as pulses [21], a CEP of 70° is chosen for the near-single-cycle ($\sim$ 3.3 fs) driving pulse. The focus of our work was to extend this strategy to few-cycle pulses with relatively long temporal durations (e.g., $\sim$ 5 fs) by adding a control

field. From a technical point of view, a $\sim$ 5-fs few-cycle pulse will be more easily generated and manipulated than a near-single-cycle 3.3 fs pulse. The new waveform-controlled two-color laser field leads to intense IAPs. The numerical simulation demonstrated that when a weak 15-fs, 1600-nm control pulse was superposed on the intense 5-fs, 800-nm main pulse and both pulses were sine waveform, the efficiency of the HHG is boosted by approximately two orders of magnitude as compared to that in the case that both pulses are cosine waveform, as shown in Fig. 11(a). In the inset of Fig. 11(a), we can clearly see that in the sine-waveform two-color field, the electrical field which ionized the electrons with the high kinetic energy upon recombination is strong, that leads to a high tunneling ionization rate as well as HHG yield. In spite of the fact that there is another trajectory that electrons can gain high kinetic energy, the ionization rate is much lower due to the broken symmetry of the driving field. In contrast, in the cosine-waveform two-color field, high-energy recolliding electron contributing to HHG is born at the moment when the electric field is relatively weak, resulting in the low HHG yield due to the high sensitivity of tunnel ionization to the laser intensity.

Temporal profiles of attosecond pulses are obtained by performing inverse Fourier transforms for the XUV supercontinua generated with sine- and cosine-waveform driving pulses, as shown in Fig. 11(b). Clearly, the intensity of attosecond pulses generated with the sine-waveform two-color pulse is almost two orders of magnitude stronger than that with the cosine-waveform pulse in the case without any phase compensation. The satellite pulses are about two orders of magnitude weaker than the main pulses. Further phase compensation using XUV chirped mirrors or metal foils with an opposite sign of dispersion slope would lead to near-transform-limited attosecond pulses with the duration of less than 50 as. Therefore, the sine-waveform two-color field offers a promising method to create intense attosecond pulses by significantly enhancing ionization rate of high-energy recolliding electron contributing to the XUV supercontinuum.

IV. CONCLUSIONS AND OUTLOOK

In this work, we have reviewed our main achievements on HHG driven by two-color laser fields. It was demonstrated that two-color field can effectively manipulate ionization, propagation and recombination processes involved in HHG due to its unique ability to control electron wavepackets on the sub-cycle time scale and the sensitivity of HHG on the pulse waveform. Both theoretical and experimental studies in the last a few years have revealed the advantages of two-color field scheme for broadening XUV supercontinuum, creating shorter IAPs, selecting single quantum trajectory, controlling wavelength, bandwidth, polarization and yield of HHG. These investigations will help to motivate the widespread use of HHG in many fields, such as attoseocond nonlinear optics, molecular imaging, nanolithography, X-ray microscopy, etc.

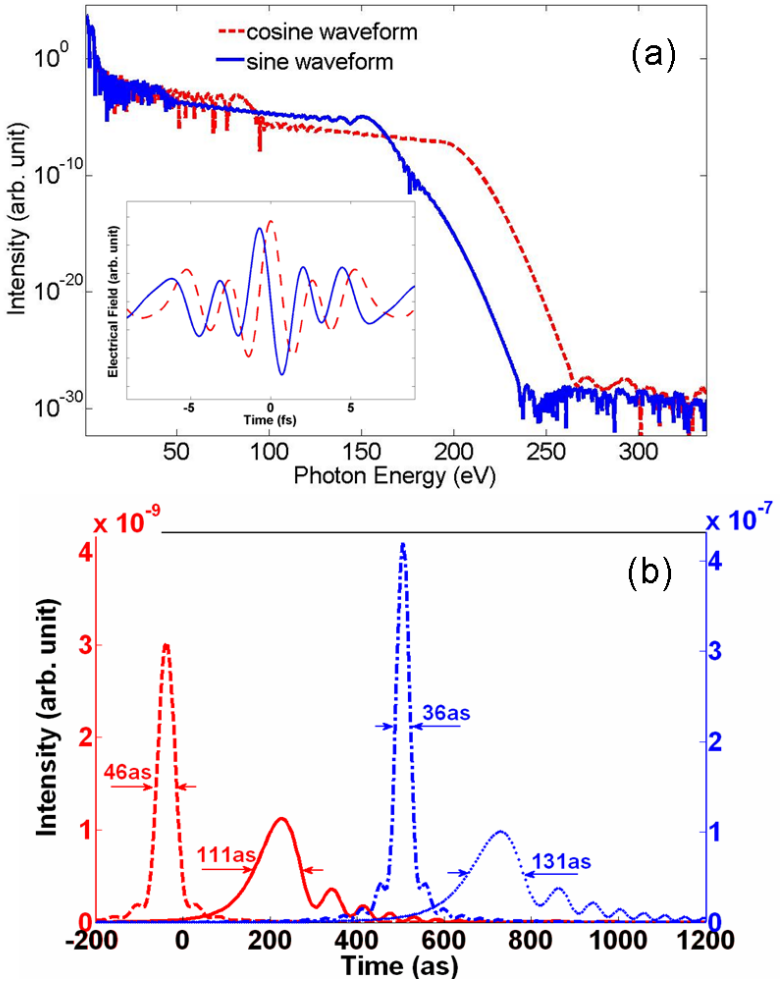

FIG. 11: (a) Comparison of HHG spectra generated in two-color driving pulses with cosine (dashed line) and sine waveforms (solid line). The corresponding electric fields are shown in inset. (b) Temporal profiles of HHG spectra generated by cosine-waveform pulses without (solid line) and with phase compensation (dashed line), by sine-waveform pulses without (dotted line) and with phase compensation (dash-dotted line).

Acknowledgements

This work is supported by the National Basic Research Program of China (Grant Nos. 2011CB808100, 2014CB921300), National Natural Science Foundation of China (Grant Nos. 11127901, 11134010, 61221064, 61275205, 11274050 and 11204332) and the Program of Shanghai Subject Chief Scientist (11XD1405500). We acknowledge the contributions of Xiaohong Song, Yongli Yu, Yuxi Fu, Hui Xiong, Han Xu, Haisu Zhang, Chenrui Jing, Hongqiang Xie *et al.*

References

[1] P. Corkum, Phys. Rev. Lett. **71**, 1994 (1993).
[2] X. Zhang *et al.*, Opt. Lett. **29**, 1357-1359 (2004).
[3] R. L. Sandberg *et al.*, Phys. Rev. Lett. **99**, 098103 (2007).
[4] M. Drescher *et al.*, Nature **419**, 803 (2002).
[5] I. J. Sola *et al.*, Nat. Phys. **2**, 319 (2006).
[6] A. D. Shiner *et al.*, Nat. Phys. **7**, 464 (2011).
[7] C. Spielmann *et al.*, Science **278**, 661 (1997).
[8] H. Xiong *et al.*, Opt. Lett. **34**, 1747 (2009).
[9] F. Krausz, Phys. World **14**, 41 (2001).
[10] J. Itatani *et al.*, Nature **432**, 867 (2004).
[11] C. Vozzi *et al.*, Nat. Phys. **7**, 822 (2011).
[12] W. Li *et al.*, Science **322**, 1207 (2008).
[13] O. Smirnova *et al.*, Nature **460**, 972 (2009).
[14] H. J. Worner, J. B. Bertrand, D. V. Kartashov, P. B. Corkum, and D. M. Villeneuve, Nature **466**, 604 (2010).
[15] T. C. Steven, J. Phys. D: Appl. Phys. **35**, R43 (2002).
[16] A. Wirth *et al.*, Science, **334**, 195 (2011).
[17] T. Pfeifer, L. Gallmann, M. J. Abel, D. M. Neumark, and S. R. Leone, Opt. Lett. **31**, 975 (2006).
[18] Y. Oishi, M. Kaku, A. Suda, F. Kannari, and K. Midorikawa, Opt. Express **14**, 7230 (2006).
[19] Z. Zeng, Y. Cheng, X. Song, R. Li, and Z. Xu, Phys. Rev. Lett. **98**, 203901 (2007).
[20] M. V. Ammosov, N. B. Delone, and V. P. Krainov, Sov. Phys. - JETP **64**, 1191 (1986).
[21] E. Goulielmakis *et al.*, Science **320**, 1614 (2008).
[22] J. Yao *et al.*, Phys. Rev. A **82**, 023826 (2010).
[23] I. J. Sola *et al.*, Nat. Phys. **2**, 319 (2006).
[24] H. Mashiko *et al.*, Phys. Rev. Lett. **100**, 103906 (2008).
[25] I. Thomann *et al.*, Opt. Express **17**, 4611 (2009).
[26] M. Lewenstein, P. Balcou, M. Ivanov, A. L'Huillier, and P. Corkum, Phys. Rev. A **49**, 2117 (1994).
[27] Z. Chang, Phys. Rev. A **71**, 023813 (2005).
[28] Y. Zheng *et al.*, Opt. Lett. **33**, 234 (2008).
[29] Y. Yu *et al.*, Opt. Express **16**, 686 (2008).
[30] C. Ruiz, D. J. Hoffmann, R. Torres, L. E. Chipperfield, and J. P. Marangos, New J. Phys. **11**, 113045 (2009).
[31] M. Lein, J. Phys. B: At. Mol. Opt. Phys. **40**, R135 (2007).
[32] Y. Yu *et al.*, Phys. Rev. A **80**, 053423 (2009).
[33] B. K. McFarland, J. P. Farrell, P. H. Bucksbaum, and M. Gühr, Science **322**, 1232 (2008).
[34] X. Feng *et al.*, Phys. Rev. Lett. **103**, 183901 (2009).
[35] Y. Niu, Y. Xiang, Y. Qi, and S. Gong, Phys. Rev. A **80**, 063818 (2009).
[36] B. Zeng *et al.*, Phys. Rev. A **85**, 033839 (2012).
[37] X. Song *et al.*, Phys. Rev. A **76**, 043830 (2007).
[38] L. B. Da Silva *et al.*, Phys. Rev. Lett. **74**, 3991 (1995).
[39] J. B. M. Warntjes *et al.*, Opt. Lett. **26**, 1463 (2001).
[40] L. Poletto *et al.*, Opt. Lett. **32**, 2897 (2007).
[41] R. Bartels *et al.*, Nature **406**, 164 (2000).
[42] X. Zhang *et al.*, Nat. Phys. **3**, 270 (2007).

[43] Z. Zeng *et al.*, Phys. Rev.A **77**, 023416 (2008).
[44] C. Zhang *et al.*, Opt. Express **20**, 16544 (2012).
[45] P. Wei *et al.*, Phys. Rev. Lett. **110**, 233903 (2013).
[46] J. Yao *et al.*, Phys. Rev. A **83**, 033835 (2011).
[47] C. Zhang *et al.*, Opt. Express **21**, 3259 (2013).
[48] E. Constant *et al.*, Phys. Rev. Lett. **82**, 1668 (1999).
[49] E. J. Takahashi, Y. Nabekawa, and K. Midorikawa, Appl. Phys. Lett. **84**, 4 (2004).
[50] I. J. Kim *et al.*, Phys. Rev. Lett. **94**, 243901 (2005).
[51] E. J. Takahashi, P. Lan, O. D. Mücke, Y. Nabekawa, and K. Midorikawa, Nat. Commun. **4**, 2691 (2013).
[52] T. Kanai, E. Takahashi, Y. Nabekawa, and K. Midorikawa, Phys. Rev. Lett. **98**, 153904 (2007).
[53] E. J. Takahashi, T. Kanai, K. L. Ishikawa, Y. Nabekawa, and K. Midorikawa, Phys. Rev. Lett. **99**, 053904 (2007).
[54] J. Chen, B. Zeng, X. Liu, Y. Cheng, and Z. Xu, New J. Phys. **11**, 113021 (2009).
[55] B. Zeng *et al.*, J. Phys. B: At. Mol. Opt. Phys. **42**, 145604 (2009).